Y and Ni Co-Doped $BaZrO_3$ as a Proton-Conducting Solid Oxide Fuel Cell Electrolyte Exhibiting Superior Power Performance

Shahid P. Shafi, Lei Bi,[z] Samir Boulfrad, and Enrico Traversa[*,z]

Division of Physical Sciences and Engineering, King Abdullah University of Science and Technology (KAUST), Thuwal 23955-6900, Saudi Arabia

The fabrication of anode supported single cells based on $BaZr_{0.8}Y_{0.2}O_{3-\delta}$ (BZY20) electrolyte is challenging due to its poor sinteractive nature. The acceleration of shrinkage behavior, improved sinterability and larger grain size were achieved by the partial substitution of Zr with Ni in the BZY perovskite. Phase pure Ni-doped BZY powders of nominal compositions $BaZr_{0.8-x}Y_{0.2}Ni_xO_{3-\delta}$ were synthesized up to x = 0.04 using a wet chemical combustion synthesis route. $BaZr_{0.76}Y_{0.2}Ni_{0.04}O_{3-\delta}$ (BZYNi04) exhibited adequate total conductivity and the open circuit voltage (OCV) values measured on the BZYNi04 pellet suggested lack of significant electronic contribution. The improved sinterability of BZYNi04 assisted the ease in film fabrication and this coupled with the application of an anode functional layer and a suitable cathode, $PrBaCo_2O_{5+\delta}$ (PBCO), resulted in a superior fuel cell power performance. With humidified hydrogen and static air as the fuel and oxidant, respectively, a peak power density value of 428 and 240 mW cm^{-2} was obtained at 700 and 600°C, respectively.

 [DOI: 10.1149/2.0701514jes]

Manuscript submitted September 8, 2015; revised manuscript received October 6, 2015. Published October 16, 2015.

The increasing worldwide energy demand and the threatening environmental pollution from conventional fossil fuel combustion call for the thrive of sustainable alternative energy supply. In the past decade, there has been a growing interest toward proton conducting ceramics owing to their high proton conductivity with low activation energies at intermediate temperatures.[1] These ceramic materials, termed as high temperature proton conductors (HTPCs), exhibit proton conductivity under hydrogen and/or steam atmospheres[2–6] and find applications as electrolyte membranes for proton conducting solid oxide fuel cells[7,8] and steam electrolyzers,[9,10] as well as hydrogen separation membranes.[11–14]

One of the major challenges for practical deployment has been the selection of an appropriate electrolyte material with adequate ionic conductivity at low temperatures, good processability, and chemical stability for long-term operation in working conditions. To date, although a wide range of proton conductor materials has been reported,[15,16] the majority of the researches on HTPC electrolytes still focus on $BaCeO_3$ and $BaZrO_3$ related materials.[17,18] Y-doped $BaCeO_3$ (BCY) exhibits good sinterability with appropriate protonic conductivity, but practical application is hindered by its reactivity with acidic gases such as CO_2 that leads to decomposition into $BaCO_3$ and CeO_2. In contrast, Y-doped $BaZrO_3$ (BZY) is chemically stable at fuel cell working conditions, but BZY poor sinterability results in large volumes of poorly conducting grain boundaries in ceramic bodies that end up in significantly reducing the total proton conductivity. Nonetheless, it has been reported that grain boundary free BZY thin films exhibit superior bulk proton conductivity.[19]

The fabrication of BZY-based cells with high ionic conductivity and dense microstructure is a major challenge. The refractory nature of $BaZrO_3$ hinders its application in fuel cells or other related devices. Typically, temperatures as high as 1700°C and long soaking times (24 h) are required to attain dense pellets. Implementations of such extreme conditions are not only costly, but also long sintering times at high temperatures can induce barium oxide evaporation leading to conductivity losses.[5] In addition, co-firing with potential electrode materials at such conditions is impeded due to potential electrode/electrolyte interface reactions and the loss of electrode porosity. Numerous sintering aids such as NiO,[20] CuO,[21] ZnO,[22] CaO[23] and $LiNO_3$[24] have been successfully used to promote the sinterability and reduce the sintering temperature of $BaZrO_3$-related electrolytes. Notably, additives such as Fe, Cr and V were detrimental to the densification behavior.[22] Another approach to promote the sinterability of $BaZrO_3$ is the substitution of Zr^{4+} with trivalent or tetravalent metal cations. $BaZrO_3$ - $BaCeO_3$ solid solutions with higher Ce-concentration showed improved sinterability, however, at the expense of the chemical stability.[25] Yttrium is considered as the most appropriate dopant for $BaZrO_3$ to obtain enhanced proton conductivity. Significantly improved sinterability was achieved by incorporating indium or gallium as a second dopant in BZY.[26] Recently, Fabbri et al. demonstrated that with Pr-doping an almost fully dense microstructure can be achieved for BZY at appropriate temperatures.[27]

Despite the improvement in the sinteractivity through the application of sintering aids in BZY, the fabrication of corresponding cells with desired power performance through conventional ceramic processes still remains a major challenge. The contribution from ohmic resistance can be minimized by using thin electrolyte films in HTPC fuel cells. An anode supported single cell based on BZY electrolyte film of 4 μm thickness fabricated via pulsed laser deposition (PLD) exhibited a peak power density of 110 mW cm^{-2} at 600°C.[28] Progress in the identification of chemically stable BZY-based electrolytes and the fabrication of corresponding single cells is highly desirable for the advancement of proton conducting SOFCs.

We report here the effect of Ni-doping in BZY with emphasis on the sinterability, stability and fuel cell performance. Previous studies did not focus on controlling the stoichiometry such that Ni is incorporated at a specific site in the BZY perovskite.[20] In the reactive sintering method, excess sintering aid is mixed (super-stoichiometrically added in wt%) with the electrolyte and this may introduce perovskite structural changes such as A-site deficiency.[6] The present study stoichiometrically targets partial substitution of Zr with Ni in the BZY perovskite. 4 mol% Ni-doped BZY (BZYNi04) exhibited adequate proton conductivity and excellent sinteractivity. Anode supported single cells with BZYNi04 electrolyte film fabricated via co-pressing method demonstrated excellent power output performance.

Experimental

Ni-doped BZY powders of $BaZr_{0.8-x}Y_{0.2}Ni_xO_{3-\delta}$ ($0.01 \leq x \leq 0.06$, BZYNi0X) compositions were prepared by using a combustion method. Stoichiometric amounts of $Ba(NO_3)_2$, $ZrN_2O_7.xH_2O$, $Y(NO_3)_3.6H_2O$ and $Ni(NO_3)_2.6H_2O$ were dissolved in deionized water. Citric acid, as a chelating agent, was added at a 2:1 molar ratio with respect to the total metal cation concentration. NH_4OH was added to the transparent solution until the pH reached 8. The solution was heated under stirring and subsequently ignited to flame. The resulting

*Electrochemical Society Fellow.
[z]E-mail: lei.bi@kaust.edu.sa; enrico.traversa@kaust.edu.sa

ash was heated to 1100°C for 6 h. Pellets of approximately 12 mm in diameter and 1 mm in thickness were prepared using this powder and were sintered at 1500°C for 10 h. During the final sintering step, the pellets were covered with respective powder bath to avoid barium evaporation.

Room temperature powder X-ray diffraction (PXRD) data were collected using a Bruker D8 Advance diffractometer equipped with Cu $K\alpha_{1,2}$ radiation. The powder diffraction data sets were analyzed via Rietveld method using FullProf.

The surface and fractured cross-section morphology of the $BaZr_{0.8-x}Y_{0.2}Ni_xO_{3-\delta}$ ($0.0 \leq x \leq 0.04$) samples was observed using a FEI-Quanta 200 scanning electron microscope (SEM).

BZYNi0X powders prepared at 1100°C were pressed into rectangular bars and the shrinkage behavior was measured from room temperature to 1500°C at 10°C min^{-1}, followed by isothermal heating for 10 h and cooling at 10°C min^{-1} in air using a dilatometer (DIL 402C, Netzsch).

Conductivity measurements were performed on a polished BZYNi04 pellet of approximately 10.6 mm in diameter and 0.74 mm in thickness. Electrochemical impedance spectroscopy (EIS) measurements were carried out at open circuit voltage in dry and wet argon atmosphere using a multichannel potentiostat (Solartron 1470E), in the 1 MHz – 0.1 Hz frequency range.

The anode support layer for the fuel cell tests was prepared using a mixture of BZY and NiO powders in a 4:6 weight ratio. Additionally, 20 wt% of starch was added to enrich the anode porosity for improved gas diffusion. The anode functional layer made of BZY and NiO in a 4:6 weight ratio was sandwiched between the anode support and the electrolyte. The co-pressed tri-layer was co-fired at 1450°C for 6 h. A composite cathode made of $PrBaCo_2O_{5+\delta}$ (PBCO) and BZY in a 7:3 weight ratio was painted on the co-fired tri-layer and subsequently fired at 1000°C for 3 h. Fuel cell tests were performed with humidified hydrogen ($\approx$ 3% H_2O) as the fuel and static air as the oxidant. The anode side was sealed with silver and two silver wire current leads were attached to each electrode. A multichannel potentiostat, VMP3 (BioLogic Co.), was used to measure the fuel cell performance. The effective area used for the single cell tested was 0.196 cm^2.

Results and Discussion

Generally, BZY shows the best protonic conductivity when Y-concentration is 20 mol% and marked decrease in conductivity is observed when Y-content is above 30 mol%.[29,30] Consequently, in this study the Y-concentration was fixed at 20 mol% and $BaZr_{0.8-x}Y_{0.2}Ni_xO_{3-\delta}$ (BZYNi) powders were synthesized using a combustion method.

Fig. 1 shows the powder X-ray diffraction (PXRD) patterns of the Ni-doped BZY powders of the corresponding pellets annealed at 1500°C for 10 hours. As can be seen in Fig. 1, phase pure BZY powders were obtained up to 4 mol% of Ni-doping. Further increase in the Ni-dopant concentration to 6 mol% resulted in the formation of a secondary phase, $BaNiY_2O_5$ – type, and the Bragg diffraction peaks corresponding to this phase are indicated with the black lines in Fig. 1. The inset in Fig. 1 represents the PXRD patterns zoomed in to the (211) reflection of the BZYNi perovskite phases to emphasize the diffraction peak shift toward higher 2θ angle with increasing the Ni concentration, which indicates a decrease in the cubic unit cell volume.

Rietveld refinements were carried out against powder X-ray diffractograms of the BZYNi powders using FullProf.[31] BZYNi crystallizes in the cubic perovskite structure in space group $Pm\bar{3}m$ (221). During the Rietveld refinement, background parameters, cubic unit cell parameter, peak shape parameter, scale factor and zero point were refined. Fig. 2 shows the Rietveld plot for the BZYNi04 powder. The unit cell dimension deduced from Rietveld refinement is plotted as a function of the Ni concentration in BZYNi, as shown in the inset in Fig. 2. Notably, the cubic unit cell parameter decreased monotonically with increasing the Ni concentration in BZYNi. This trend is consistent with the substitution of larger Zr^{4+} (r = 0.72 Å) with smaller Ni^{2+} (r = 0.69 Å) in the 6-fold coordination.[32] Additionally, the y-axis intercept of the unit cell parameter (up to x = 0.04) linear fit (4.2286 (6) Å) is in agreement with the value reported previously for undoped $BaZr_{0.8}Y_{0.2}O_{3-\delta}$.[33] The unit cell parameter for BZYNi06 deviated from the linear trend, as shown in Fig. 2 inset, which is anticipated due to the formation of the secondary phase.

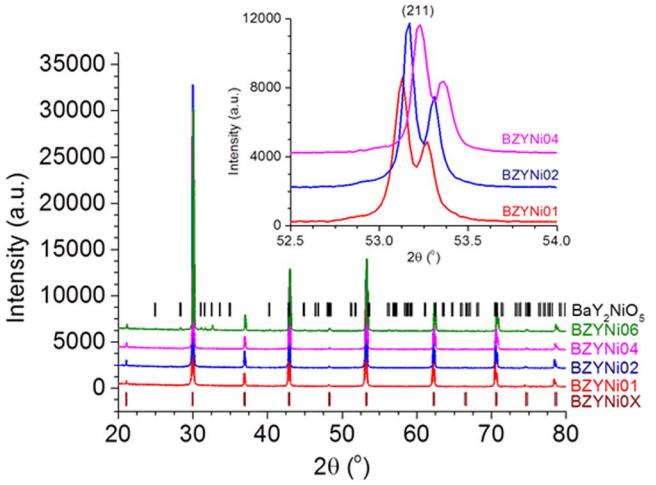

Figure 1. Powder X-ray diffraction patterns of $BaZr_{0.8-x}Y_{0.2}Ni_xO_{3-\delta}$ powders of corresponding pellets heated to 1500°C for 10 hours in air. The Bragg positions corresponding to BZYNi0X and the secondary phase $BaNiY_2O_5$ are indicated by brown and black tick marks, respectively. The PXRD patterns of BZYNi01, BZYNi02 and BZYNiO04 powders zoomed in to (211) reflection is shown in the inset.

Dilatometric measurements were carried out to follow the sintering behavior of the Ni-doped BZY pellets. Fig. 3 shows the shrinkage behavior of BZYNi and undoped BZY pellet samples. The samples were heated at 10°C min^{-1} to 1500°C followed by isothermal heating for 10 hours and then cooled down at a rate of 10°C min^{-1}. The shrinkage of all the samples initiated at approximately 1100°C: however, the shrinkage trend was accelerated for the Ni-doped samples in comparison to that of the undoped BZY. The final shrinkage for undoped BZY, 1, 2, and 4 mol% Ni-doped BZY were 21.4, 28.8, 32.5, and 34.6%, respectively. The sinteractivity of BZY has been improved considerably with increasing the Ni-dopant concentration within the solubility limit of Ni in BZY.

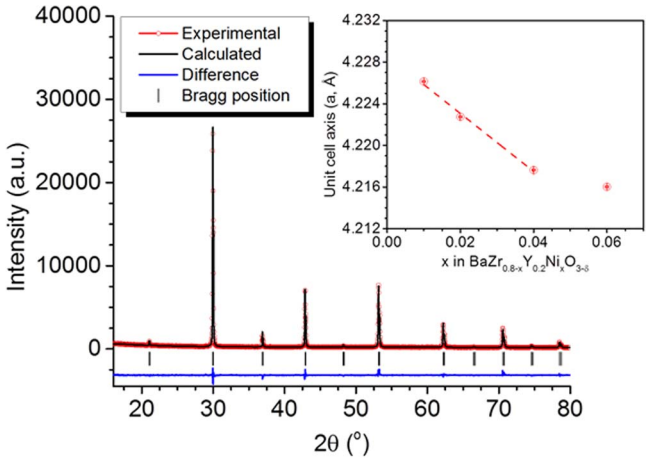

Figure 2. Rietveld plot of $BaZr_{0.76}Y_{0.2}Ni_{0.04}O_{3-\delta}$ PXRD pattern measured at room temperature. The inset illustrates the correlation of the cubic unit cell axis parameter with the Ni concentration in BZYNi.

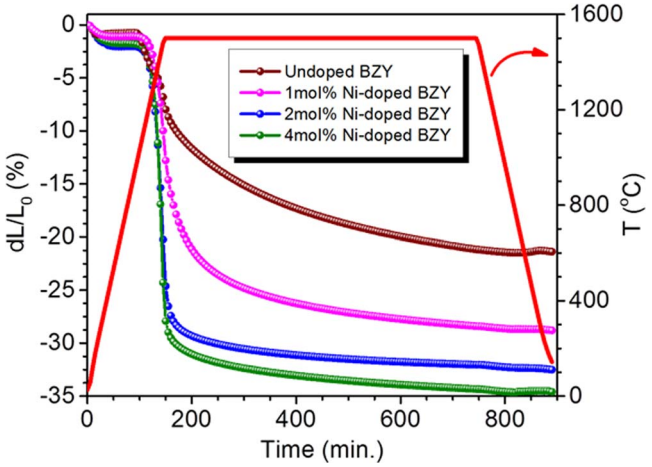

Figure 3. Dilatometric curves of pristine BZY and doped BZY with different Ni concentrations.

The surface (Figs. 4a–4d) and the fractured cross-section (Figs. 4e–4h) microstructure of undoped and Ni-doped BZY pellets sintered at 1500°C for 10 hours was investigated using scanning electron microscopy (SEM). As shown in Fig. 4, undoped BZY has a porous microstructure, whereas Ni-doping in BZY yields to a denser microstructure. As can be seen in Figs. 4b–4d, Ni-doping enhanced the grain growth significantly and the grain size increased with increasing the Ni content. The estimated average grain size (average distance between the grain boundaries) was around 0.5, 0.6 and 1.7 μm for 1, 2 and 4 mol% Ni-doped BZY, respectively. An almost completely pore-free microstructure was attained for 4 mol% Ni-doping in BZY.

Given the microstructure results, electrochemical and fuel cell tests were performed on BZYNi04, due to the better densification and large grain size. Fig. 5a shows the Arrhenius plots of the conductivity for BZYNi04 sintered at 1500°C measured in wet and dry argon. At temperatures below 650°C, the total conductivity in wet Ar was larger than that in dry Ar, which is a characteristic of proton conducting oxides. The Arrhenius plots in wet and dry Ar atmosphere merged at 700°C which can be attributed to water desorption at elevated temperatures. BZYNi04 showed a total conductivity value of 0.004 and 0.008 S cm^{-1} at 600 and 700°C, respectively, in wet Ar. The activation energy observed for the Arrhenius plots measured in wet and dry argon were 0.62 and 0.87 eV, respectively. The lower activation energy in humidified condition compared to dry atmosphere indicates that BZYNi04 is predominantly a proton conductor in the former atmosphere, and oxygen-ion and electron-hole are the main charge carriers in the latter atmosphere. Fig. 5b shows the Arrhenius plot of the BZYNi04 pellet total conductivity under fuel cell conditions and the activation energy observed was 0.67 eV, which is close to the value obtained for the BZYNi04 pellet measured in wet Ar atmosphere. The open circuit voltage (OCV) values measured across the sintered BZYNi04 pellet using platinum electrodes, with humidified hydrogen (≈ 3% H_2O) at the anode part and static air at the cathode part, were 1.03, 1.02, 1.01, 0.99, and 0.96 V at 500, 550, 600, 650, and 700°C, respectively. Assuming there is no substantial gas leakage;

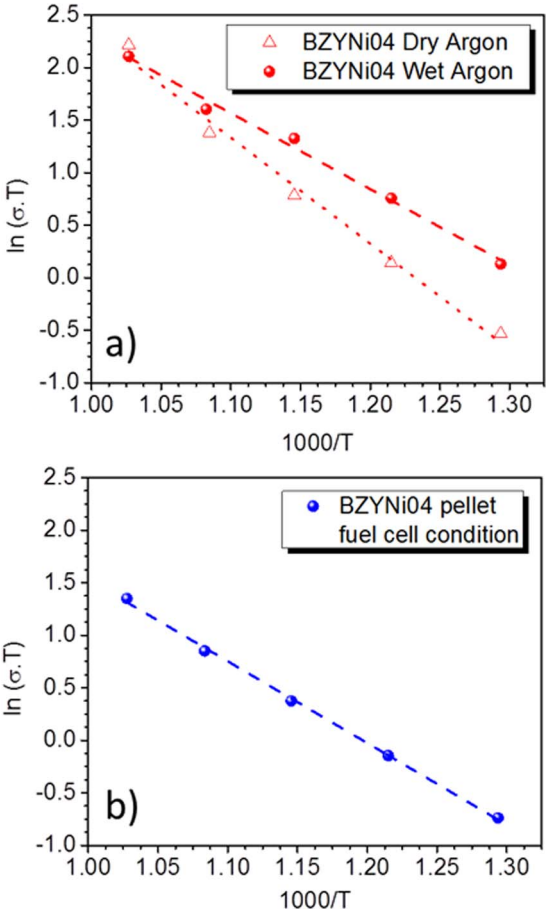

Figure 5. Arrhenius plots of the total conductivity of BZYNi04 pellets (a) in wet and dry argon, and (b) under fuel cell conditions.

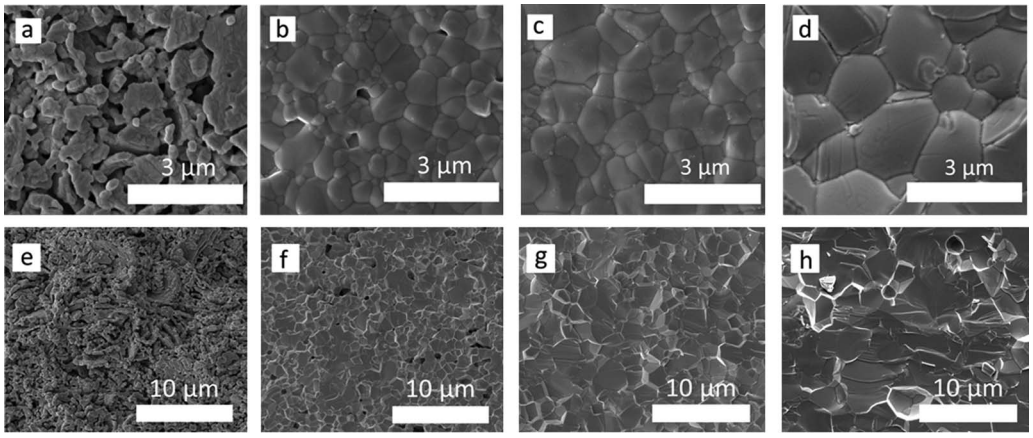

Figure 4. SEM images of the surface (TOP) and fractured cross-section (BOTTOM) morphology of (a, e) undoped BZY, (b, f) BZYNi01, (c, g) BZYNi02, and (d, h) BZYNi04 pellets sintered at 1500°C for 10 hours.

the estimated ionic transport number at 600°C is 0.91 by considering the Nernst potential. No significant electronic contribution can be observed even when the Ni concentration reaches 4 mol%. An earlier work suggested that electronic conduction can be introduced while using NiO as a sintering aid in BZY.[22] However, negligible electronic conduction is evidenced here as demonstrated from our OCV study, suggesting that the controlled addition of Ni at the B-site within the Ni solubility limit in BZY might be an effective strategy for improving the sinterability while avoiding undesirable electronic conduction for the electrolyte material.

Anode supported single cells were fabricated via co-pressing and co-firing process to evaluate the fuel cell performance of the BZYNi04 electrolyte. In order to obtain larger triple phase boundary regions and reduced electrode polarizations, composite electrodes were used.[34] The anode support and the anode functional layers consisted of BZY and NiO powders in 4:6 weight ratio and the anode support was made more porous for easy gas diffusion by adding starch prior to the co-pressing and co-firing. Single cells containing $PrBaCo_2O_{5+\delta}$ (PBCO) based composite electrode deployed with doped BZY electrolytes have shown impressive power output performances[35,36] and consequently, a composite mixture of PBCO and BZY in 7:3 weight ratio was chosen as the cathode in this study. Fig. 6a shows the I-V and power density curves for the single cell based on the BZYNi04 electrolyte, measured at various operating temperatures. The OCV values of the cell reached 0.91, 0.96, 0.99, 1.01 and 1.02 V at 700, 650, 600, 550 and 500°C, respectively, and are comparable with those obtained for BZY based single cells reported in the literature.[37,38] The high OCV values indicate the dense nature of the BZYNi04 electrolyte membrane (12 μm in thickness) allowing for no gas leakage. Applying humidified hydrogen (≈ 3% H_2O) as the fuel and static air as the oxidant, a maximum power density of 428, 340, 240, 160 and 94 mW cm^{-2} was obtained at 700, 650, 600, 550 and 500°C, respectively. Recently, Sun et al. demonstrated power performance of 360 and 379 mW cm^{-2} at 700°C for single cells based on $BaZr_{0.7}Sn_{0.1}Y_{0.2}O_{3-\delta}$ (12 μm in thickness)[38] and $BaZr_{0.8}Y_{0.15}In_{0.05}O_{3-\delta}$ (12 μm in thickness)[37] electrolyte, respectively. It should be emphasized that, to the best of our knowledge, the power performance obtained in this study is one of the best reported thus far for thermodynamically stable $BaZrO_3$-based proton conducting SOFCs, and is compared with the recent literature reports as shown in Fig. 6b.[24,27,35–37,39–43] A very recent work by C. Duan et al. suggests that the application of a proton, oxygen ion, and electron-hole conducting cathode material, $BaCo_{0.4}Fe_{0.4}Zr_{0.1}Y_{0.1}O_{3-\delta}$, combined with a novel cell fabrication method involving a reduced-temperature firing step (1400°C) can significantly improve the power output performance of BZY-based cells prepared using Ni as a sintering aid.[43] This implies that there is scope for further improvement of BZYNi04-based cell performance by employing a more appropriate cathode or cell fabrication method. In Fig. 6c, the power performance obtained in this work is compared with that in the recent literature reports focusing on Zr and Y co-doped $BaCeO_3$-based proton conducting SOFCs.[44–48] The performance reported here is comparable or superior to that of many $BaCeO_3$-based proton conducting SOFCs.[17,44,45] There are a few reports in the literature on $BaCeO_3$-based P-SOFCs with remarkable performance, as shown in Fig. 6c.[46–48] However, the inherent chemically unstable nature of $BaCeO_3$-based materials, demonstrated by many previous studies,[25,27,49–51] warrants further works to be carried out on chemically stable $BaZrO_3$-based P-SOFCs for practical applications.

Fig. 7a shows the typical electrochemical impedance plot of the BZYNi04-based fuel cell measured at 600°C under open circuit voltage. The high frequency intercept with the real axis represents the ohmic resistance (R_{ohm}), which arises mainly from electrolyte resistance, while the difference between the high and low frequency intercepts with the real axis represents the polarization resistance (R_p) of the cell. R_{ohm} was 0.27, 0.41, 0.56, 0.81, and 1.17 Ω cm^2 and R_p was 0.07, 0.10, 0.25, 0.67, and 1.79 Ω cm^2 at 700, 650, 600, 550, and 500°C, respectively, as shown in Fig. 7b. R_{ohm} is the dominating contribution toward the total resistance at temperatures higher than 550°C, and consequently reducing the electrolyte thickness could enhance the cell power performance. Based on the ohmic resistance values and the electrolyte film thickness, the film conductivity of BZYNi04 electrolyte under fuel cell conditions can be estimated: the estimated conductivity of BZYNi04 film was about 4.4×10^{-3}, 2.9×10^{-3}, 2.1×10^{-3}, 1.5×10^{-3} and 1.0×10^{-3} S cm^{-1} at 700, 650, 600, 550, and 500°C, respectively. It should be emphasized that the BZYNi04 film conductivity values under fuel cell conditions are among the best reported for BZY-related films prepared using conventional ceramic processes[23,27,36,38,39] and such high film conductivity should have helped to achieve a high fuel cell power output.

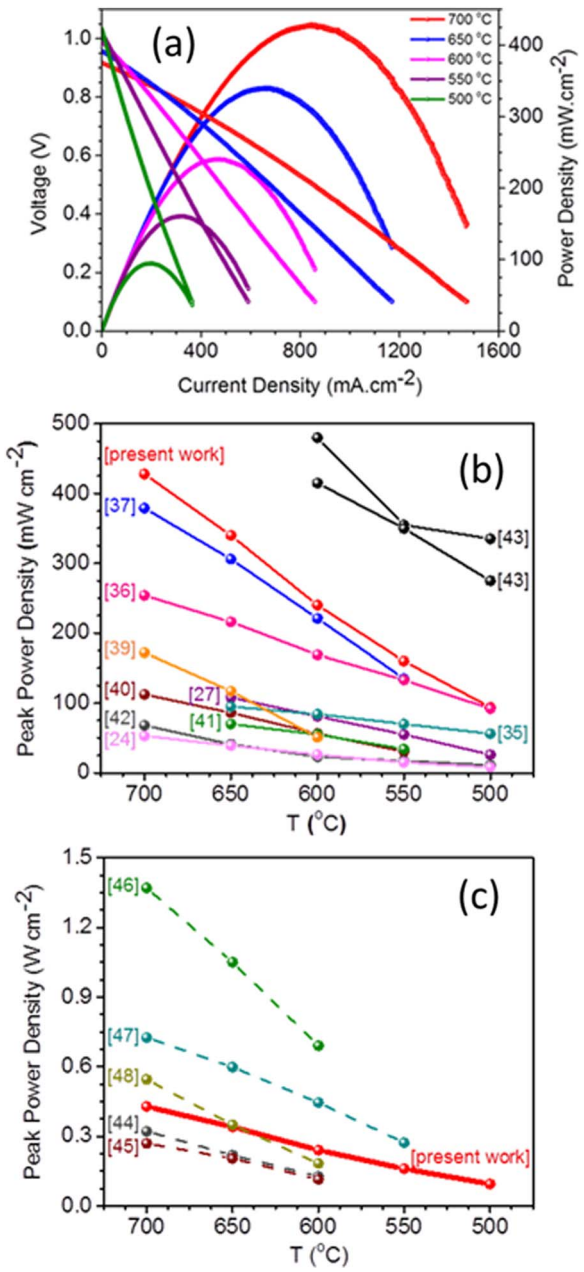

Figure 6. (a) *I-V* and power density curves of $BaZr_{0.76}Y_{0.2}Ni_{0.04}O_{3-\delta}$-based single cell measured from 500 to 700°C using humidified hydrogen (≈ 3% H_2O) as the fuel and static air as the oxidant. (b, c) Comparison of peak power density values as a function of the temperature of various $BaZrO_3$-based (b) and Zr and Y co-doped $BaCeO_3$-based (c) proton conducting fuel cells reported in the literature. The numbers correspond to the references.

Fig. 8 shows the SEM micrograph of the BZYNi04-based single cell cross-section after fuel cell testing. As can be seen in Fig. 8, the four-layer cell structure comprises a porous cathode layer, a dense

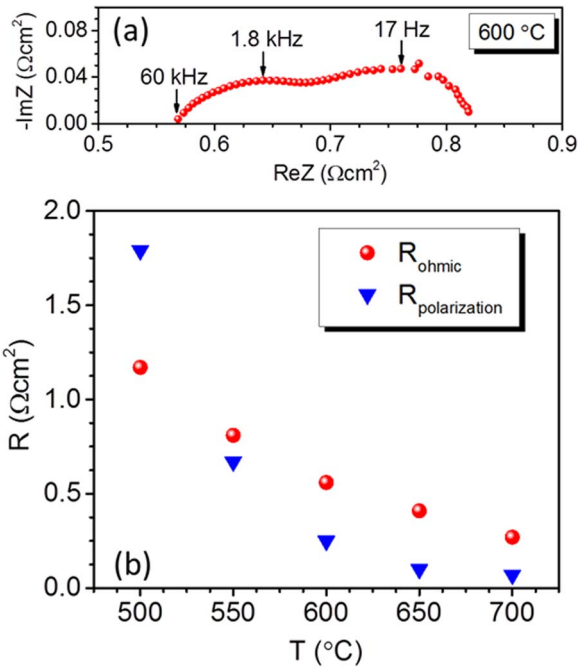

Figure 7. (a) The typical electrochemical impedance plot of BZYNi04-based fuel cell measured at 600°C under open circuit voltage. (b) The ohmic resistance and polarization resistance estimated from the impedance plots recorded during the BZYNi04 film based fuel cell test.

electrolyte membrane, a relatively less porous anode functional layer and a very porous anode support (about 0.6 mm). The fairly porous anode support allows the smooth diffusion of the fuel gas while the relatively less porous anode functional layer provides more active sites for electrochemical reactions by enhancing the triple phase boundary sites.[52] The excellent electrochemical power output obtained for this single cell indicates that the cell configuration is good for mass and charge transport in the cell. Fig. 8 inset shows a large magnification view of the electrolyte layer and the approximately 12 μm thick BZYNi04 electrolyte membrane is dense and almost free of any pores.

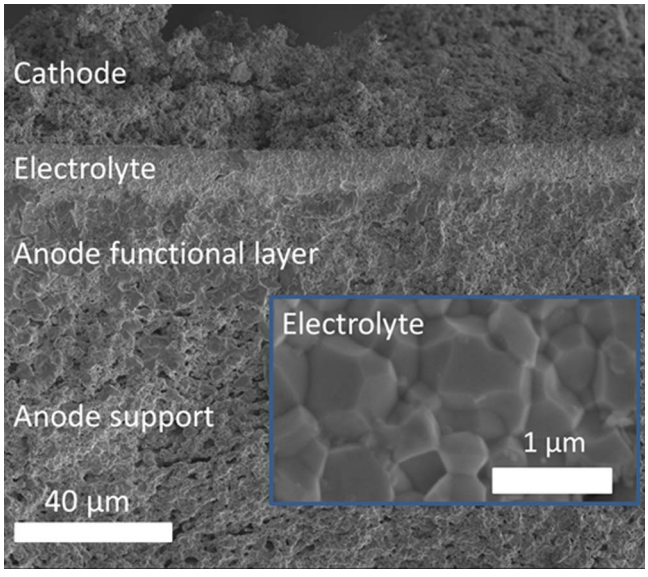

Figure 8. SEM micrograph of the BZYNi04-based single cell cross-section after fuel cell testing. The inset shows a large magnification view of the electrolyte layer.

Additionally, the contact between the electrolyte and electrode layers is very good resulting in an enhanced power output of the cell.

Conclusions

The deployment of intermediate temperature proton conducting SOFCs requires the use of chemically-stable electrolytes, which have been actively searched by our group in the last decade. This implies avoiding the use of Ce in our formulations and of non-volatile sintering additives. Here we present the development of $BaZr_{0.76}Y_{0.2}Ni_{0.04}O_{3-\delta}$ as an electrolyte membrane for P-SOFCs. The strategy of Ni-doping in the BZY lattice improved the sinterability, allowing for a dense electrolyte microstructure. Single cells fabricated on a BZY-NiO anode support with a $PrBaCo_2O_{5+\delta}$ – BZY composite cathode exhibited an excellent electrochemical power output performance. The peak power density values of 428 and 240 mW cm^{-2} were measured at 700 and 600°C, respectively.

Acknowledgments

The authors thank KAUST Advanced Imaging and Characterization Laboratories for the access to XRD and SEM facilities.

References

1. E. Fabbri, D. Pergolesi, and E. Traversa, *Chem. Soc. Rev.*, **39**, 4355 (2010).
2. H. Iwahara, T. Esaka, H. Uchida, and N. Maeda, *Solid State Ionics*, **3-4**, 359 (1981).
3. K. D. Kreuer, *Annu. Rev. Mater. Res.*, **33**, 333 (2003).
4. R. Haugsrud and T. Norby, *Nat. Mater.*, **5**, 193 (2006).
5. E. Fabbri, A. Magrasó, and D. Pergolesi, *MRS Bull.*, **39**, 792 (2014).
6. S. Tao and J. T. S. Irvine, *Adv. Mater.*, **18**, 1581 (2006).
7. H. Iwahara, *Solid State Ionics*, **28**, 573 (1988).
8. H. Iwahara, H. Uchida, and K. Morimoto, *J. Electrochem. Soc.*, **137**, 462 (1990).
9. P. A. Stuart, T. Unno, J. A. Kilner, and S. J. Skinner, *Solid State Ionics*, **179**, 1120 (2008).
10. L. Bi, S. Boulfrad, and E. Traversa, *Chem. Soc. Rev.*, **43**, 8255 (2014).
11. C. Zuo, S. E. Dorris, U. Balachandran, and M. Liu, *Chem. Mater.*, **18**, 4647 (2006).
12. S. Fang, L. Bi, X. Wu, H. Gao, C. Chen, and W. Liu, *J. Power Sources*, **183**, 126 (2008).
13. S. Fang, K. S. Brinkman, and F. Chen, *J. Membrane Sci.*, **467**, 85 (2014).
14. S. Fang, S. Wang, K. S. Brinkman, and F. Chen, *J. Mater. Chem. A*, **2**, 5825 (2014).
15. T. Omata and S. Otsuka-Yao-Matsuo, *J. Electrochem. Soc.*, **148**, E252 (2001).
16. Y. Kawasaki, S. Okada, N. Ito, H. Matsumoto, and T. Ishihara, *Mater. Res. Bull.*, **44**, 457 (2009).
17. C. Zuo, S. Zha, M. Liu, M. Hatano, and M. Uchiyama, *Adv. Mater.*, **18**, 3318 (2006).
18. E. Fabbri, L. Bi, D. Pergolesi, and E. Traversa, *Adv. Mater.*, **24**, 195 (2012).
19. D. Pergolesi, E. Fabbri, A. D'Epifanio, E. Di Bartolomeo, A. Tebano, S. Sanna, S. Licoccia, G. Balestrino, and E. Traversa, *Nat. Mater.*, **9**, 846 (2010).
20. J. Tong, D. Clark, M. Hoban, and R. O'Hayre, *Solid State Ionics*, **181**, 496 (2010).
21. D. Gao and R. Guo, *J. Alloys Compd.*, **493**, 288 (2010).
22. P. Babilo and S. M. Haile, *J. Am. Ceram. Soc.*, **88**, 2362 (2005).
23. Z. Sun, E. Fabbri, L. Bi, and E. Traversa, *J. Am. Ceram. Soc.*, **95**, 627 (2012).
24. Z. Sun, E. Fabbri, L. Bi, and E. Traversa, *Phys. Chem. Chem. Phys.*, **13**, 7692 (2011).
25. E. Fabbri, A. D'Epifanio, E. Di Bartolomeo, S. Licoccia, and E. Traversa, *Solid State Ionics*, **179**, 558 (2008).
26. N. Ito, H. Matsumoto, Y. Kawasaki, S. Okada, and T. Ishihara, *Solid State Ionics*, **179**, 324 (2008).
27. E. Fabbri, L. Bi, H. Tanaka, D. Pergolesi, and E. Traversa, *Adv. Funct. Mater.*, **21**, 158 (2011).
28. D. Pergolesi, E. Fabbri, and E. Traversa, *Electrochem. Commun.*, **12**, 977 (2010).
29. K. D. Kreuer, St. Adams, W. Munch, A. Fuchs, U. Klock, and J. Maier, *Solid State Ionics*, **145**, 295 (2001).
30. E. Fabbri, D. Pergolesi, S. Licoccia, and E. Traversa, *Solid State Ionics*, **181**, 1043 (2010).
31. J. Rodriguez-Carvajal, FullProf. 2k, Vers. 4.40; (2008).
32. R. D. Shannon, *Acta Crystallogr.*, **A32**, 751 (1976).
33. Y. Yamazaki, R. Hernandez-Sanchez, and S. M. Haile, *J. Mater. Chem.*, **20**, 8158 (2010).
34. E. Fabbri, D. Pergolesi, and E. Traversa, *Sci. Tech. Adv. Mater.*, **11**, 044301 (2010).
35. L. Bi, E. Fabbri, Z. Sun, and E. Traversa, *Solid State Ionics*, **196**, 59 (2011).
36. L. Bi, E. Fabbri, Z. Sun, and E. Traversa, *Energy Environ. Sci.*, **4**, 409 (2011).
37. W. Sun, Z. Shi, M. Liu, L. Bi, and W. Liu, *Adv. Funct. Mater.*, **24**, 5695 (2014).
38. W. Sun, M. Liu, and W. Liu, *Adv. Energy Mater.*, **3**, 1041 (2013).
39. L. Bi, E. Fabbri, Z. Sun, and E. Traversa, *Energy Environ. Sci.*, **4**, 1352 (2011).
40. Y. Ling, F. Wang, L. Zhao, X. Liu, and B. Lin, *Electrochimica Acta*, **146**, 1 (2014).
41. J. Xiao, W. Sun, Z. Zhu, Z. Tao, and W. Liu, *Mater. Lett.*, **73**, 198 (2012).
42. Y. Liu, R. Ran, M. O. Tade, and Z. Shao, *J. Membrane Sci.*, **467**, 100 (2014).
43. C. Duan, J. Tong, M. Shang, S. Nikodemski, M. Sanders, S. Ricote, A. Almansoori, and R. O'Hayre, *Science*, **349**, 1321 (2015).

44. Z. Tao, L. Bi, L. Yan, W. Sun, Z. Zhu, R. Peng, and W. Liu, *Electrochem. Commun.*, **11**, 688 (2009).
45. F. Zhao and F. Chen, *Int. J. Hydrogen Energy*, **35**, 11194 (2010).
46. J. Kim, S. Sengodan, G. Kwon, D. Ding, J. Shin, M. Liu, and G. Kim, *ChemSusChem*, **7**, 2811 (2014).
47. L. Yang, C. Zuo, S. Wang, Z. Cheng, and M. Liu, *Adv. Mater.*, **20**, 3280 (2008).
48. L. Zhao, B. He, B. Lin, H. Ding, S. Wang, Y. Ling, R. Peng, G. Meng, and X. Liu, *J. Power Sources*, **194**, 835 (2009).
49. K. Katahira, Y. Kohchi, T. Shimura, and H. Iwahara, *Solid State Ionics*, **138**, 91 (2000).
50. K. H. Ryu and S. M. Haile, *Solid State Ionics*, **125**, 355 (1999).
51. S. Tao and J. T. S. Irvine, *Adv. Mater.*, **18**, 1581 (2006).
52. L. Bi, E. Fabbri, and E. Traversa, *Electrochem. Commun.*, **16**, 37 (2012).